A new approach to measure border irregularity for melanocytic lesions

Tim K. Lee[a,b] and M. Stella Atkins[b*]

[a] BC Cancer Agency, Vancouver, BC, Canada, V5Z 4E6
[b] Simon Fraser University, Burnaby, BC, Canada, V5A 1S6

ABSTRACT

One of the important clinical features to differentiate benign melanocytic nevi from malignant melanomas is the irregularity of the lesion border. A careful examination of a lesion border reveals two types of irregularity: texture irregularity and structure irregularity. Texture irregularities are the small variations along the border, while structure irregularities are the global indentations and protrusions, which may suggest excess of cell growth or regression of a melanoma. Therefore, measuring border irregularity by structural indentations and protrusions may detect the malignancy of the lesion. The common shape descriptors such as compactness index and fractal dimension are more sensitive to texture irregularities than structure irregularities. They do not provide an accurate estimation for the structure irregularity. Therefore, we have designed a new measurement for border irregularity. The proposed method first locates all indentations and protrusions along the lesion border. Then a new area-based index, called irregularity index, is computed for each indentation and protrusion. The overall border irregularity is estimated by the sum of all individual indices. In addition, the new method offers an extra feature: localization of the significant indentations and protrusions. As the result, the new measure is sensitive to structure irregularities and may be useful for diagnosing melanomas.

Keywords: medical image analysis, melanoma, shape, border irregularity, scale space filtering.

1. INTRODUCTION

Cutaneous malignant melanoma incidence has been increasing in all Western countries for many years.[1] Early diagnosis is crucial to the treatment process because the survival rate is inversely proportional to the thickness of the lesion.[2] Several recent research studies have investigated early detection methods using computer image analysis techniques.[3-12] These studies utilized the lesion clinical features such as lesion shape, colour and size to differentiate benign nevi from malignant melanomas. Among these features, border irregularity has been reported as the most significant factor in clinical diagnosis[13]. Clinically, malignant melanomas are often described as having a jagged and scalloped border, while melanocytic nevi have a circumscribed, round or oval contour.[14, 15] Histologically, indentations and protrusions along the lesion border may suggest regression of a melanoma or excess of cell growth. Therefore, estimating border irregularity accurately is important for computerizing early detection method. To measure border irregularity, many studies used some of the well-known shape descriptors, such as compactness index[3-7] or fractal dimension[8-11].

Claridge et al.[8] reported that there are two types of irregularities: texture and structure irregularities. Texture irregularity is the fine variation along the lesion border that is sensitive to noise, while the structure irregularity is the general undulations of the perimeter that are related to major indentations and protrusions. These indentations and protrusions are important diagnostic features for melanomas. Claridge et al. pointed out that estimating the structure fractal dimension is more important than the overall fractal dimension and texture fractal dimension of the lesion border.

In our previous paper published in SPIE 1999 Medical Imaging Conference,[16] we reported a new measure, called sigma-ratio, for border irregularity. Sigma-ratio is derived from scale-space filtering technique. When a lesion border is continuously convolved by a Gaussian kernel with an increasing σ, the indentations and protrusions along the border are smoothed-out in order. The minimum σ required to eliminate all indentations and protrusions, with an appropriate normalization, is defined as sigma-ratio, which can be used as an indicator of the roughness of the lesion border. We have shown that sigma-ratio is more sensitive to structure irregularity than compactness index, overall fractal dimension and structure fractal dimension. However, there are some shortcomings for sigma-ratio. First, it is sensitive to a long and narrow

* Further author information: (Send correspondence to Tim K. Lee.)
Tim K. Lee: E-mail: tlee@bccancer.bc.ca
M. Stella Atkins: E-mail: stella@cs.sfu.ca

In *Medical Imaging 2000: Image Processing*, Kenneth M. Hanson, Editor,
Proceedings of SPIE Vol. 3979 (2000) • 1605-7422/00/$15.00

indentation such as the phantom shown in Fig. 1. For example, when an occluding hair of a skin lesion is misinterpreted as an indentation, the sigma-ratio has a very high value. Hence, sigma-ratio requires all hairs to be shaved or to be removed by a software preprocessor DullRazor[17]. Secondly, sigma-ratio is non-linear due to the non-linear property of the Gaussian smoothing process.

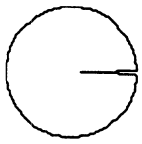

Figure 1. A phantom.

In this paper, we extended sigma-ratio to a new area-based measurement, called irregularity index, by directly locating and measuring the indentations and protrusions along the lesion border.

2. METHOD

2.1. Definition of Indentations and Protrusions

It is common to locate the tip of an indentation or a protrusion by computing the local extrema of the curvature of a curve.[18-20] The calculation can be carried out on a lesion border when the border is abstracted as a closed planar curve. Further simplification can be made by parameterization of the x and y coordinates into two linear functions x(t) and y(t), where t is the path length variable along the planar curve.[21] The curvature function of the curve contains a lot of information. The sign indicates concavity or convexity of the curve segment and the magnitude denotes the amount of bending. A local curvature extreme marks the tip of a concavity or a convexity. Because we have to compute the extent of an indentation and a protrusion, in this paper, an indentation is defined as a segment of the curve that begins with a convex curvature extreme, followed by a concave curvature extreme and ending with a convex curvature extreme. Similarly, a protrusion can be defined as a curve segment that begins with a concave curvature extreme, followed by a convex curvature extreme and ending with a concave extreme. (See Fig. 2.) However, curvature calculation is a local operation that results in texture irregularities only.

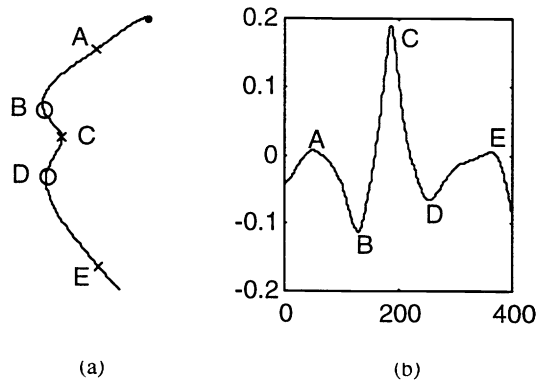

Figure 2. (a) A curve segment running from top to bottom with the figure at the left-hand side. There are two protrusions and one indentation on the curve segment. (b) The curvature function of the curve segment shown in (a). The local extrema are located and marked with A, B, C, D and E. The corresponding locations are shown in (a) too. The protrusions and indentation are defined by the curvature local extrema. From the definition, the two protrusions are the curve segments [A B C] and [C D E], while the indentation is the curve segment [B C D].

2.2 Global Structure Extraction

Convolution with a Gaussian filter is a well-known smoothing technique in computer vision to extract global structure. The scale-space theory showed that a Gaussian filter is the only convolution kernel that satisfies the 'causality' property of filtering.[22] In other words, no new irregularities, indentations or protrusions, will be generated as artifacts during a continuous smoothing process and irregularities are smoothed out gradually in a 'proper' order. Small irregularities will disappear before larger ones. When some indentations or protrusions are smoothed out, at their places may emerge a larger indentation or protrusion. The larger irregularity is considered as the 'global' irregularity for the smaller 'local' ones. Hence, a hierarchical structure for irregularities is formed. See Fig. 3 for a demonstration of the Gaussian smoothing process. A lesion border is smoothed by an increasing σ until all indentations and protrusions are eliminated.

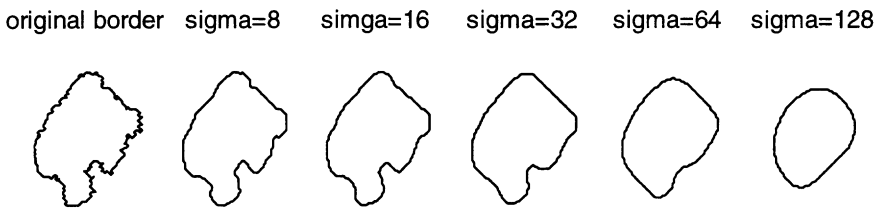

Figure 3. Gaussian smoothing process of a lesion border.

Unfortunately, Gaussian smoothing also distorts the shape of the curve and the locations of any feature, such as the locations of the local curvature extrema. Scale-space theory solves the distortion problem by proposing a 2-D scale-space image.[21, 23] For the current application, the scale-space image needs to be extended from a binary image to a three-valued image to encode the local concavity or convexity property of the curve segment. Such an extended three-valued scale-space image for Fig. 3 is constructed and shown in Fig. 4. The y-axis of the image represents the smoothing scale that is denoted by Gaussian σ, and the x-axis represents the spatial position of the investigated feature, the local extreme positions of the curvature values. At any smoothing scale σ, the zero-crossings of the first derivative of the curvature values are recorded as

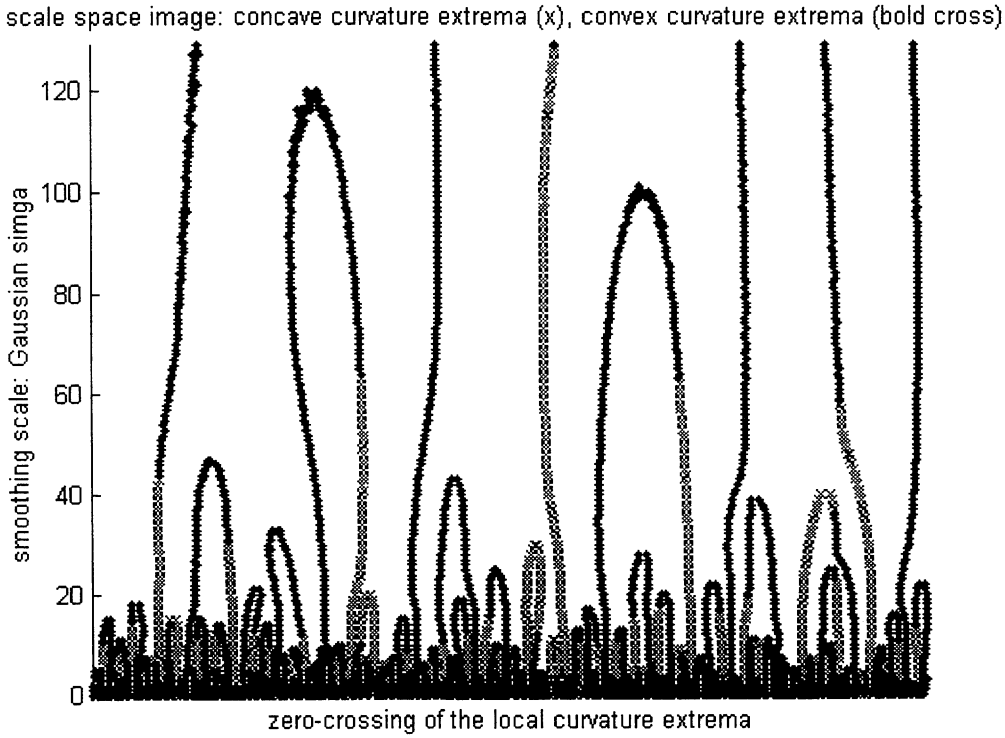

Figure 4. The extended scale-space image for Gaussian smoothing process shown in Fig. 3.

points on the image along with the concavity or convexity property of the local curve segment. Therefore, from the extended scale-space image, we can identify all indentation and protrusion segments using the definition in Sect. 2.1. In particular, an indentation/protrusion segment is denoted by three consecutive curvature extrema with alternating signs. By examining the σ levels sequentially, all indentation and protrusion segments for the entire smoothing process can be recorded.

Furthermore, with coarse-to-fine tracking, the actual locations of the found indentation and protrusion segments can be tracked and mapped back to the zero-scale, the original non-smoothed curve. Once the mapping to the original curve is established, we can prune the same indentation and protrusion segments found at different σ levels. For any two segments at $\sigma 1$ and $\sigma 2$, where $\sigma 1 > \sigma 2$, the two segments are considered the same segment if they are mapped to the same zero-scale segment. The segment at a lower level, $\sigma 2$, can be deleted. The mapping can also capture the hierarchical structure of the indentation and protrusion segments. When a larger segment covers the locations of several smaller indentation/protrusion segments at lower σ levels, the larger segment can be considered as the 'global' segment for the smaller 'local' segments.

The extended scale-space image can determine other properties of an indention/protrusion segment. Every such segment has a formation σ level and a smooth-out σ level. The formation level indicates when the segment first appears, while the smooth-out level indicates when the segment is smoothed-out and disappears. When a segment is formed, we have to ensure that it is not a 'flat' irregularity segment. Specially, a segment is denoted by three consecutive curvature extrema with alternating signs. When the absolute magnitude of the middle curvature extremum or the maximum absolute magnitude of the first and the last curvature extremum is smaller than certain threshold and very close to zero, the newly formed segment is an insignificant 'flat' indentation/protrusion segment. Such a segment is removed from further computation. For this paper, the threshold is set to 0.01.

In summary, by analyzing the extended scale-space image, we can identify all global and local indentation and protrusion segments in a hierarchical structure. Each segment has an associated position on the original lesion border and a smooth-out σ level.

2.3. Irregularity Index

For each indentation/protrusion segment, an index is required to measure its severity. One way is to observe the smoothing effect on the segment. When an indentation and a protrusion is smoothed-out, the indentation and protrusion is partially filled or removed. The size of the affected area depends on the severity of the irregularity. A 'larger' indentation/protrusion requires 'more' smoothing power, and, hence, more areas are affected. Therefore, the index of severity can be measured by comparing the area difference between the smoothed segment at the smooth-out σ level and the original non-smoothed segment. For example, Fig. 5a shows a lesion border and a smoothed border at the smooth-out σ level for the largest indentation at the bottom of the figure. The shaded area indicates the filling done by the smoothing process. Likewise, Fig. 5b shows the same lesion and the smoothed border for the most prominent protrusion at the bottom of the figure. The shaded area demonstrates the removed area by the smoothing process.

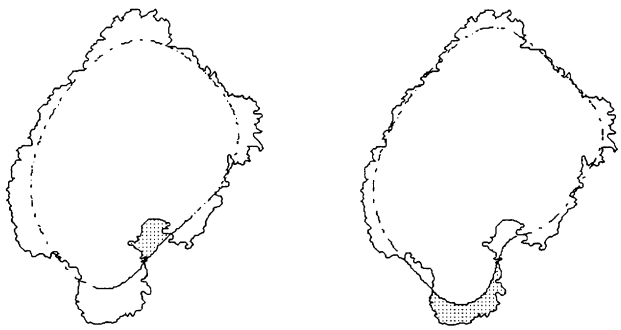

Figure 5. (a) A lesion border is shown by the solid line, while the smoothed curve corresponding to the smooth-out σ level for the largest indentation is shown by the dashed line. The shaded area denotes the area filled by the smoothing process. (b) The smoothed curve corresponding to the smooth-out σ level for the largest protrusion is shown by the dashed line. The removed area by the smoothing process is marked by the shaded area.

The index for each indentation and protrusion segment should be normalized so that it can be used for comparison among different lesion borders. Normalization can be achieved by dividing by the area of the original non-smoothed curve or the smoothed curve at the corresponding smooth-out σ level. The latter is chosen to put more weight on the larger indentation/protrusion segment, which has a smaller smoothed curve. Therefore, an irregularity index is defined for each indentation/protrusion segment as the ratio of the area difference for the segment between the smoothed segment at the smooth-out σ level and the original non-smoothed segment over the area of the smooth-out curve.

Because the indentation/protrusion segments are in a hierarchical structure, the 'local' indentation/protrusion segments can be folded into their global counterparts so that the smaller local segments can be removed. We are careful not to double count the shared irregularity areas of the local and global segments during the folding process. Now we have a set of measurements for all global indentation/protrusion segments, from which many other important parameters about a lesion border can be inferred. In particular, two important descriptors representing the border irregularity can be derived. The most significant irregularity index ranks all individual indices and indicates the largest indentation or protrusion segment of the border, while the overall irregularity index represents the entire lesion shape by summing all individual indices.

3. RESULTS AND DISCUSSION

The described methodological development has been implemented in Matlab and tested on the selected images from our skin image database. These images were collected from the patients referred to the Pigmented Lesion Clinics in Vancouver, BC, Canada. They were RGB colour images digitized from a hand-held video microscopy camera using a 20 times magnification lens. Each image contained 486 x 512 pixels with the spatial resolution of 25μm x 33μm. Before the images could be used for the feasibility test, they were processed by two automatic preprocessing programs to extract the lesion border contour. First, the skin image was checked against dark thick hairs. These hairs were removed using a software program called DullRazor[17] to reduce interference with the automated segmentation program. Then the lesion border contour was extracted automatically.[24] Ideally the two processing steps should be combined so that the segmentation program would recognize the black thick hairs and the lesion simultaneously. The combined method, however, would over-complicate the segmentation program due to the fact that hairs may divide the lesion into many sub-parts. Joining all sub-parts together to form a single lesion again would be a non-trivial task.

To demonstrate the new algorithm, the lesion border shown in Fig. 5 is used. Fig. 6 shows 15 indentation and protrusion segments found by the algorithm with their associated irregularity indices sorted in descending order. The top left-hand subfigure depicts the most significant protrusion with the highest irregularity index of 4.2, while the next subfigure illustrates the largest indentation of the lesion with an index of 2.4. The overall irregularity index for this lesion border is 15.1.

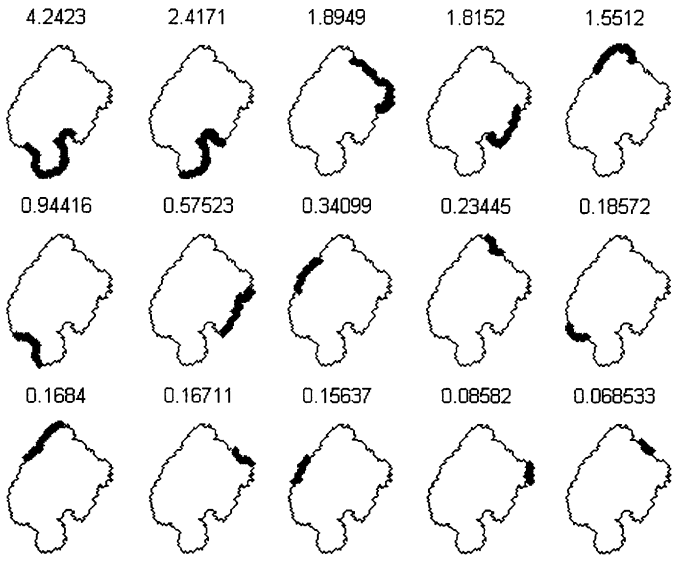

Figure 6. Fifteen indentation and protrusion segments for Fig. 5 are plotted. The subfigures are sorted by their individual irregularity index, which is reported at the top of the subfigure. The corresponding indentation/protrusion segment is highlighted along the border.

Fig. 7 reports the most significant irregularity with their associated index for two other lesion borders. The lesion on the left-hand side has the overall irregularity index of 6.8 and the most significant index of 3.3. These two indices suggest that there is a significant protrusion in the lesion; otherwise, the lesion border is relatively smooth. On the other hand, the lesion border in the right-hand side has the overall irregularity index of 6.3; but the most significant irregularity index of 0.4 implies there is no major indentation and protrusion, but a fair amount of texture irregularity.

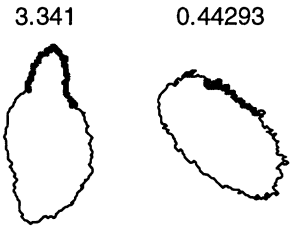

Figure 7. The algorithm results for two others borders. The largest irregularity segment is highlighted and the corresponding irregularity index is reported at the top of the lesion border. The overall irregularity index for the left-hand subfigure and the right-hand subfigure are 6.8 and 6.3, respectively.

Fig. 8 compares our new indices, overall irregularity index and most significant irregularity index, with other shape descriptors such as the overall fractal dimension, structure fractal dimension and compactness index using the three lesion borders. The compactness index is sensitive to texture irregularity. The middle subfigure has fewer texture irregularities than the other two subfigures. Therefore, the middle subfigure has the smallest compactness index of 2.3. Furthermore, the compactness index is not sensitive to the presence of the prominent indentation and protrusion in the left-hand subfigure. Its compactness index of 4.1 is almost identical to the right-hand subfigure, which has no significant structure indentation and protrusion. Similar situation occurs for the overall fractal dimension and the structure fractal dimension. They both fail to recognize the prominent indentation and protrusion in the left-hand subfigure. On the other hand, our method of measuring irregularity indices identifies all indentations and protrusions on the lesion border. Each irregularity is carefully analyzed independently. Hence, our measures provide an accurate description of each lesion border. The new measures are sensitive to structure irregularities in the left-hand and the middle subfigures. Also, the texture irregularities in the right-hand subfigure can be inferred too. Furthermore, our algorithm not only returns the overall and the most significant irregularity indices, but also returns a set of measurements for all global indentation and protrusion segments. (See Fig. 6.) This rich set of data can be used to infer other border properties. For example, the number of 'large' or 'medium' irregularities can be numerated. The new measurement set describes fully the complexity of the lesion border.

Compactness index	4.1	2.3	4.2
Overall fractal dimension	1.12	1.07	1.16
Structure fractal dimension	1.21	1.17	1.28
Overall irregularity index	15.1	6.8	6.3
Most significant irregularity index	4.2	3.3	0.4

Figure 8. Comparison of shape descriptors used for measuring border irregularity.

Unlike our previous descriptor sigma-ratio, the new measures, the overall and the most significant irregularity indices, are area-based. Therefore, the non-linearity problem reported in Sect 1. can be avoided. Furthermore, the overall irregularity index for the phantom shown in Fig. 1 is 0.4 that reflects the small size of the indentation. (See Fig. 9.) The new algorithm is less sensitive to the hair problem and missing a hair by the preprocessor DullRazor does not cause a big problem.

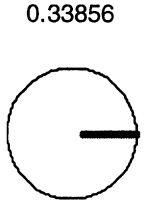

Figure 9. The most significant indentation is highlighted for the phantom shown in Fig. 1. The associated most significant irregularity index is shown at the top of the figure. The overall irregularity index is 0.4.

Another advantage of the irregularity index is that it can pinpoint and highlight a potential problem area of the lesion border (see Fig. 7) and explain the final measurement by its individual sub-components (see Fig. 6). Physicians can verify the highlighted irregularities and their indices before making the final diagnosis. This detailed information provided by the new measure will be more useful than other 'black-box' styled single value measurements such compactness index and fractal dimension.

Even though the irregularity index was developed and implemented for melanocytic lesions, it can also be applied to other medical related problems, such as differentiating the malignancy of other solid tumors. Furthermore, since the formation of the methodology depends only on a planar closed curve, it can be used as a shape descriptor for other general 2-D image analysis problems. For example, it can be used to identify the largest bay (the most significant indentation) on an aerial map.

4. CONCLUSION

We have designed and implemented a new measure called irregularity index for melanocytic lesion border irregularity. The major advantage of the new measure is that it directly locates indentations and protrusions along the lesion border. Using an extended scale-space image as the intermediate data representation, we numerate all irregularities and compute the associated indices. This set of measurements provides a rich description for the lesion border. We further examined two measurements derived from the set, the overall irregularity index and the most significant irregularity index. Comparing the new measurements with other shape descriptors, namely, compactness index, overall fractal dimension, and structural fractal dimension, we found that the overall irregularity index and the most significant irregularity index are more sensitive to the structure irregularity than other shape descriptors. Therefore, the new measurements may be useful for diagnosing melanomas.

ACKNOWLEDGMENTS

This work was supported in part by a BC Health Research Foundation grant #142(97-2).

REFERENCES

1. B.K. Armstrong, D.R. English, "Cutaneous malignant melanoma," in *Cancer Epidemiology and Prevention*, D. Schottenfeld, J. F. Fraumeni Jr., eds., pp. 1282-1312, Oxford University Press, New York, 1996.
2. C. M. Balch, A. Houghton, L. Peters, "Cutaneous melanoma," in *Cancer Principles and Practice of Oncology*, V. T. DeVita Jr., S. Hellman, S. A. Rosenberg., eds., J.B. pp. 1499-1542, Lippincot Company, Philadelphia, 1989.
3. R. White, D. S. Rigel, R Friedman, "Computer applications in the diagnosis and prognosis of malignant melanoma," *Dermatologic Clinics* **9**, pp. 695-702, 1992.
4. J. E. Golston, W. V. Stoecker, R. H. Moss, I.P.S. Dhillon, "Automatic detection of irregular borders in melanoma and other skin tumors," *Computerized Medical Imaging and Graphics* **16**, pp. 199-203, 1992.
5. F. Ercal, A. Chawla, W. V. Stoecker, H. C. Lee, R. Moss, "Neural network diagnosis of malignant melanoma from color images," *IEEE Trans Biomed Eng* **41**, pp. 837-45, 1994.
6. W. V. Stoecker, R. Moss, F. Ercal, S. Umbaugh, "Nondermatoscopic digital imaging of pigmented lesions," *Skin Res Technol* **1**, pp. 7-16, 1995.
7. O. Colot, R. Devinoy, A. Sombo, D. de Brucq, "A color image processing method for melanoma detection," in *Proceedings of the First International Medical Imaging Computing and Computer-Assisted Intervention*, pp. 562-569, Cambridge, 1998.

8. E. Claridge, P. N. Hall, M. Keefe, J. P. Allen, "Shape analysis for classification of malignant melanoma," *J Biomed Eng* **14**, pp. 229-234, 1992.
9. P.N. Hall, E. Claridge, J. D. Morris, "Computer screening for early detection of melanoma- is there a future?" *Br J Dermatol* **132**, pp. 325-338, 1995.
10. V. Ng, T. Lee, "Measuring border irregularities of skin lesions using fractal dimensions," in *SPIE Photonics China, Electronic Imaging and Multimedia Systems* **2898**, pp. 64-72, Beijing, 1996.
11. E. Claridge, J.D. Morris Smoth, P.N. Hall, "Evaluation of border irregularity in pigmented skin lesions against a consensus of expert clinicians," in *Medical Image Understanding and Analysis*, Leeds, U.K., 1998.
12. Image and signal based analysis of pigmented skin lesions, *British Machine Vision Association Technical Meeting, London 18 March 1998*, http://www.cs.bham.ac.uk/~exc/Research/BMVA_mtg.html.
13. M. Keefe, D. Dick, R. Wakeel, "A study of the value of the seven-point checklist in distinguishing benign pigmented lesions from melanoma," *Clinical Experimental Dermatol* **15**, pp. 167-171, 1990.
14. J. K. Rivers, "Melanoma," *Lancet* **347**, pp. 803-807, 1996.
15. J. C. Maize, A. B. Ackerman, *Pigmented Lesions of the Skin*, Philadelphia, Lea & Febiger, 1987.
16. T. Lee, S. Atkins, R. Gallagher, C. MacAulay, A. Coldman, D. McLean, "Describing the structural shape of melanocytic lesions," in *Image Processing, Proc. SPIE* **3661**, pp. 1170-1179, San Diego, 1999.
17. L. Lee, V. Ng, R. Gallagher, A. Coldman, D. McLean, "DullRazor: a software approach to hair removal from images," *Comput Biol and Med* **27**, pp. 533-543, 1997.
18. H. Asada and M. Brady, "The curvature primal sketch," *IEEE Trans. Pattern Analysis and Machine Intelligence* **8**, pp. 2-14, 1983.
19. W. Richards and D. D. Hoffman, "Condon constraints on closed 2D shapes," *Computer Vision, Graphics, and Image Processing* **31**, pp. 265-281, 1985.
20. M. Leyton, "A process-grammar for shape," *Artificial Intelligence* **34**, pp. 213-247, 1988.
21. F. Mokhtarian, "Silhouette-based isolated object recognition through curvature scale space," *IEEE Trans. on Pattern Analysis and Machine Intelligence* **17**: pp. 539-544, 1995.
22. T. Lindeberg. *Scale-space Theory in Computer Vision*, Kluwer Academic Publishers, Boston, 1994.
23. A.P. Witkin, "Scale space filtering," in *Proceedings of the 8th International Joint Conference of Artificial Intelligent*, pp. 1019-1022, 1983.
24. T. Lee, V. Ng, D. McLean, A. Coldman, R. Gallagher, J. Sale, "A multi-stage segmentation method for images of skin lesions," in *Proceedings of IEEE Pacific Rim Conference on Communications, Computers and Signal Processing*, pp. 602-605, Victoria, British Columbia, 1995.